Modeling Capabilities for Part Distortion Management for Machined Components

T. D. Marusich , D. A. Stephenson, S. Usui, S. Lankalapalli
Third Wave Systems, Inc, 7900 West 78th St. Suite 300, Minneapolis, MN 55439
dave.stephenson@thirdwavesys.com

Abstract
Residual stresses and part distortion have a major cost impact in many machining applications since they can affect scrap rates and processing times. For example, in aerospace monolithic structures they may produce distortions which hamper assembly operations.

Residual stresses in machined components arise both from the primary process in the parent workpiece (rolling, forging, etc.) and from different plastic deformation and thermal gradients induced by machining itself. There has been significant research on predicting machining-induced residual stress, but little work on the effects of both bulk and machining-induced stresses on part accuracy.

This paper presents a comprehensive framework for predicting part distortions based on both bulk and machining-induced residual stresses. Machining induced stresses are computing using a three-dimensional FEM model which includes fully adaptive unstructured mesh generation, tight thermo-mechanical coupling, deformable tool-chip-workpiece contact, momentum effects at high speeds, constitutive models appropriate for high strain rate, and finite deformation analysis. Application of these stresses and corresponding measured bulk stresses in a complete part-level analysis, using a toolpath analysis program, is discussed. Preliminary results of the part distortion prediction capability are presented for a T-section part and two large structural thin-walled components.

1. INTRODUCTION

Residual stresses in the part have a significant quality and cost impact in many machining operations. This is particularly true for large airframe and similar components, since strains induced by residual stresses may lead to significant distortion. This can lead to a high scrap rate for some components, and to extended machining times if material is removed in multiple light passes to control distortion.

Residual stresses in machined parts result from two sources. Prior to machining, bulk stresses from primary processes such as rolling or forging may be present in the workpiece. Superimposed on these are residual stresses induced by the machining process, which result from differential plastic deformation and surface temperature gradients [1]. Significant distortions can arise from both sources, particularly in thin-walled parts.

There has been considerable research on predicting machining-induced residual stresses, most recently using finite elements methods [2-7]. Predictions of the most advanced models are qualitatively accurate (with respect to the shape of the subsurface stress distribution and the influence of major input variables); given the difficulty of repeatably measuring residual stresses, model predictions are as reliable as unrepeated measurements in many cases. There has been little work, however, on predicting distortion in a machined structure due to bulk residual stresses from a primary process, although as noted above distortions from this source are often significant in thin-walled structures.

This paper describes an integrated approach to predicting distortions in machined structures due to both bulk and machining-induced residual stresses. Previously reported work on predicting machining-induced residual stresses through finite element modeling is briefly reviewed in Section 2. In Section 3, the integration of theses stresses into a toolpath analysis program which also takes into account bulk

stresses to predict distortions is described. Preliminary comparison of analytical predictions with measurements for airframe components are reviewed in Section 4. Section 5 summarizes conclusions are areas for further research.

2. FINITE ELEMENT CALCULATION OF MACHINING INDUCED RESIDUAL STRESSES

For this research, machining residual stresses were calculated using AdvantEdge™, an explicit dynamic, thermo-mechanically coupled finite element model specialized for metal cutting. Features necessary to model metal cutting accurately include adaptive remeshing capabilities for resolution of multiple length scales such as cutting edge radius, secondary shear zone and chip load; multiple body deformable contact for tool-workpiece interaction, and transient thermal analysis. A comprehensive discussion on the numerical techniques was and validation examples are available in the literature [8,9].

In order to model chip formation, constitutive modeling for metal cutting requires determination of material properties at high strain rates, large strains, and short heating times and is quintessential for prediction of segmented chips due to shear-localization [10,11]. Specific details of the constitutive model used are outlined in [8]. The model contains deformation hardening, thermal softening and rate sensitivity tightly coupled with a transient heat conduction analysis appropriate for finite deformations.

Machining-induced residual stresses are computed by thermo-mechanically relaxing the workpiece after machining. After the tool passes, thermo-mechanical computations are continued until transient thermal gradients in the machined surface dissipate and the work sample comes an equilibrium configuration with a resultant residual stress distribution.

3. INTEGRATING BULK AND MACHINING INDUCED RESIDUAL STRESSES

To determine the effects of both machining induced and bulk residual stresses on distortion of a machined structure, an approach combining FEA results with toolpath-level analysis is required. Fig. 1 show the approached used in this research. The Tool Path Analysis component, adapted from the AdvantEdge Production Module, a commercially available mechanistic model for 5-axis end milling [12], reads in the initial workpiece geometry, tool path, workpiece material properties, and generates the final geometry of the workpiece. The Distortion Prediction component generates a mesh of the final geometry of the workpiece, builds a finite element model, imposes bulk stresses and residual stresses from machining onto the model and performs an equilibrium analysis. Results of predicted workpiece distortions are displayed through a visualization tool.

The Toolpath Analysis component is based on well known mechanistic modeling approaches and will not be described. The modules that make up the Distortion Prediction component are described in the following.

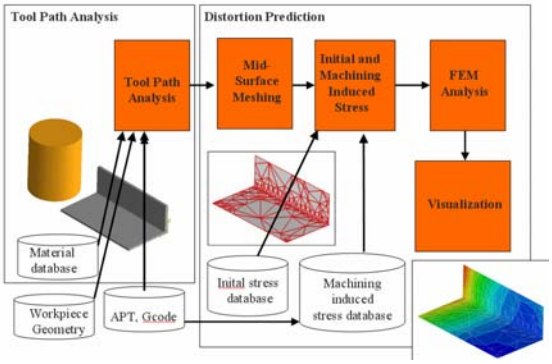

Fig. 1: Approach to modeling distortion

Workpiece Meshing

Using existing methods for toolpath generation and Boolean subtraction of workpiece material along toolpath, the final geometry of the thin-walled workpiece is generated. From the final geometry, a shell mesh is generated.

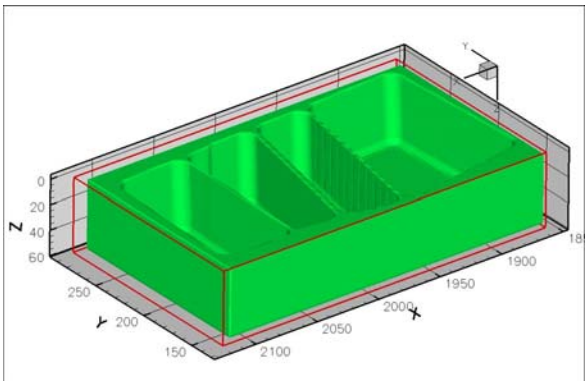

Fig. 2: Solid Model of four pocket part

A typical part for illustrating this procedure is shown in Fig. 2. In this part all ribs are perpendicular to the XY plane, but can taper in the Z-direction.

The thin-walled workpieces are modeled by a mesh of triangular shell elements. The solution is obtained by implicit methods.

Explicit stiffness matrix expressions for plate element are used where all stiffness matrix computations are done in a local coordinate system defined for each element. With reference to Fig. 3, the origin of the local coordinate system is located at node 1. The local X-axis is defined by the unit vector ($\mathbf{e}_{12}$) along a line connecting node 1 to node 2.

The unit vector along local Z axis ($\mathbf{e}_z$) is obtained by taking the cross product of $\mathbf{e}_{12}$ and $\mathbf{e}_{13}$, where $\mathbf{e}_{13}$ is the unit vector along a line connecting node 1 to node 3. Finally, unit vector along local Y axis ($\mathbf{e}_y$) is obtained by taking the cross product of $\mathbf{e}_z$ and $\mathbf{e}_{12}$.

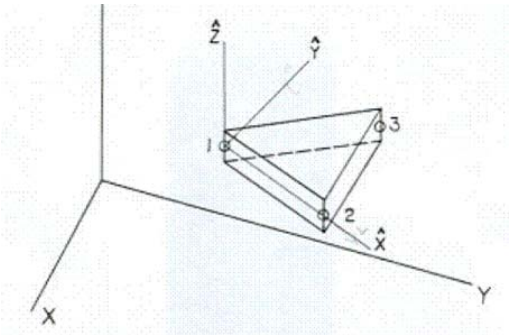

Fig. 3: Local and Global coordinate systems

The rearranged stiffness matrix is transformed to global coordinate system and assembled into the global stiffness matrix.

Fig. 4 shows a section of typical thin-walled components to be analyzed. The geometry consists of ribs (walls), webs (flanges) and fillets. Ribs are subjected to machining induced stresses from side cutting whereas webs are subjected to machining induced stresses from end milling. In general, the fillet region is small compared to the cross-section of the component. As a first approximation, it may be assumed that stress in the fillet regions do not contribute significantly to the overall distortion of the part. With this, the mapping task simplifies to determining procedures for wall and rib mapping.

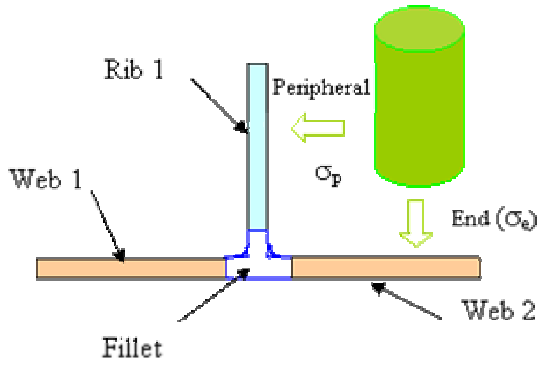

Fig. 4: Typical thin-walled section

Machining induced stresses for different process conditions, computed through finite element calculations as discussed above, are stored in a machining induced stress database. The database consists of machining induced stress profiles (Fig. 5) as function of the cutting speed, feed rate, depth of cut, tool nose radius, and radial and axial rake angles.

Fully three-dimensional stress profiles on the machined surface can be stored.

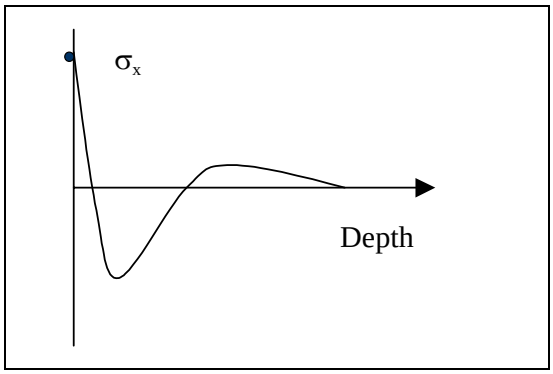

Fig. 5: Typical machining induced stress profile

The toolpath is used to obtain the solid model of the final geometry of the workpiece. The machining induced stress mapping is performed on the surface of the thin-walled workpiece. Residual stresses are determined from the database with process parameters computed the workpiece surface and applied to the corresponding element in the mesh. Nodal forces in the element due to applied residual stresses are computed and stored to be used later in the assembly of the global RHS vector. Nodal

forces from residual stresses are computed and stored for all elements on the surface.

Bulk stresses from the primary process are incorporated in an analogous manner. Limited published data for these profiles is available in the literature; a typical example is shown in Fig. 6 [13]. These stresses are applied to the mesh in a manner analogous to that used for the machining induced stresses.

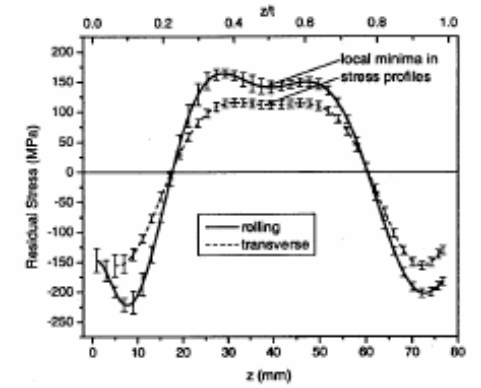

Fig. 6: Residual stresses in 80 mm thick 7050 T74 Al plate [13]

Once the stresses are applied, assembly of the global stiffness matrix, global right hand side (RHS) vector and application of boundary conditions are done using standard Finite Element techniques.

4. PRELIMINARY APPLICATION TO AEROSPACE COMPONENTS

Analyses were carried out for two aerospace structural parts provided by EADS, the fillet rib and pressure bulkhead shown in Figs. 7 and 8. Both the parts are made of Al7050 and have several pockets, thin walls of different thicknesses, and 5-axis walls.

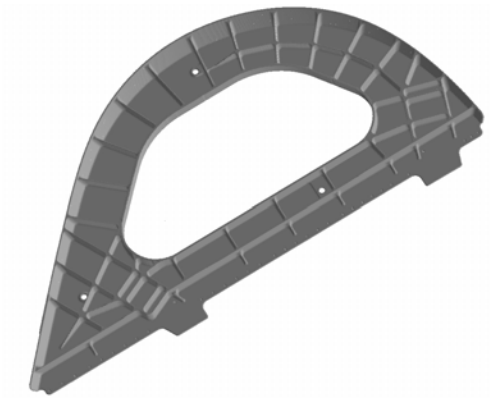

Fig. 7: Fillet Rib (1.51 m x 785mm x 38mm)

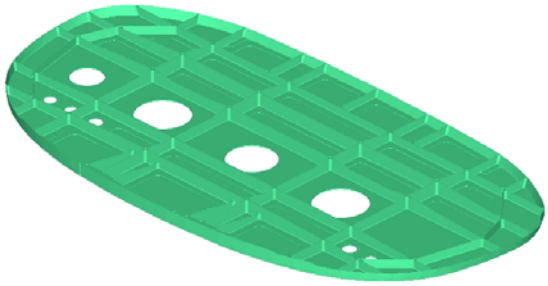

Fig. 8: Pressure Bulkhead (1.63m x 3.14m x 76mm)

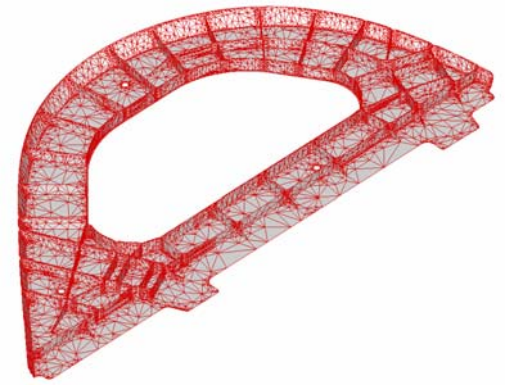

Fig. 9: Mesh for fillet rib.

The mesh for the fillet rib, which contains 22,736 elements and was automatically generated, is shown in Fig. 9. This part is machined from a rectangular block of dimensions 1.62 m x 900mm x 60mm. Distortions computed are shown in Fig. 10. CMM measurements of distortions from a machined component, taken at the points illustrated in Fig. 11, are shown in Fig. 12. Fig. 13 shows the comparison between the measured and predicted distorted shapes. As can be seen, the measured and predicted distortions agree well both qualitatively and quantitatively in this case.

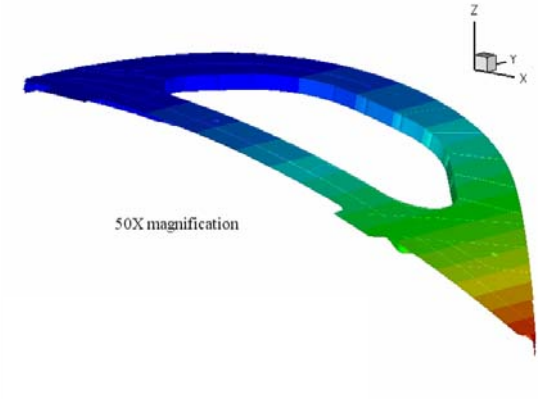

Fig. 10: Predicted distorted shape of Fillet Rib

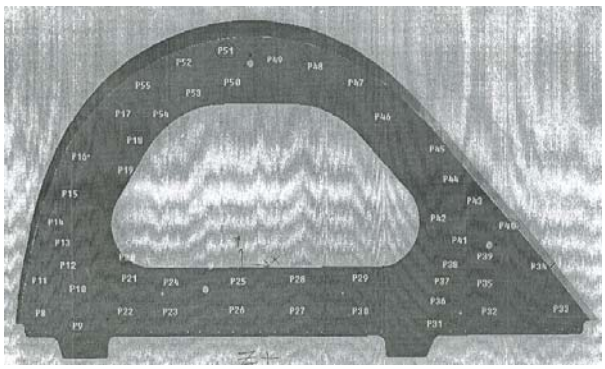

Fig. 11: Locations at which distortion was measured by CMM

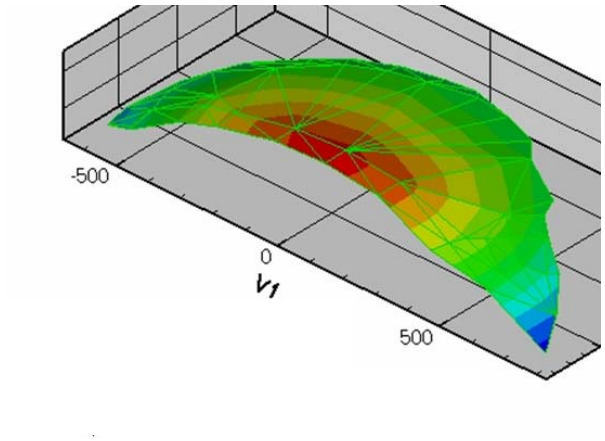

Fig. 12: Surface plot of measured distortion

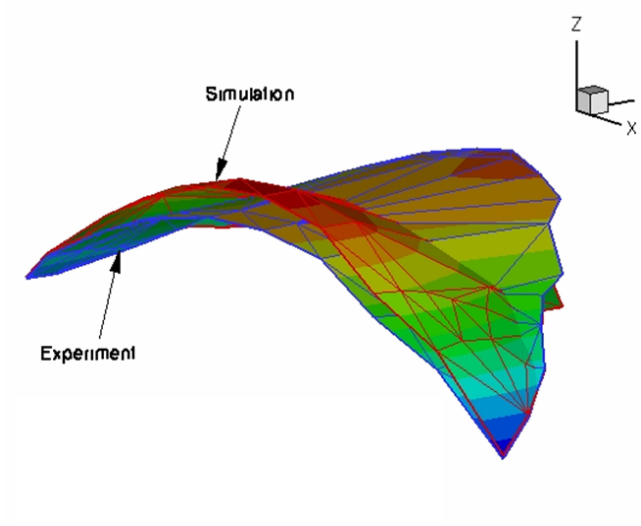

Fig. 13: Comparison of computed and measured distortions for the fillet rib.

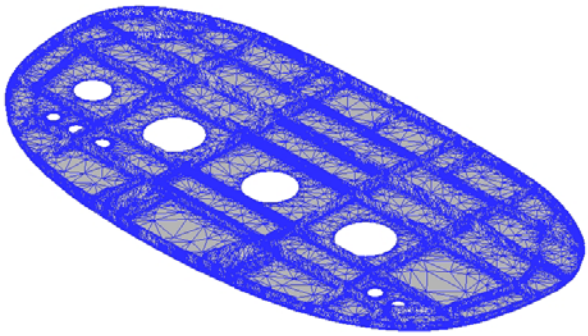

Fig. 14: Pressure Bulkhead mesh of 147,769 elements

The mesh for the pressure bulkhead, which contains 147,769 elements, is shown in Fig. 14. The Pressure Bulkhead was machined from a rectangular block of dimensions 3.33 m x 1.82 m x 100mm. The final part is located 10.0 mm from the bottom of rectangular block. Distortion of the component after machining was measured at several points (see Fig. 15) on the bottom flange along the circumference using feeler gauges. The measured distortion profile is shown in Fig. 16, and a comparison of predicted and measured distortions is shown in Fig. 21. In this case, the measured and computed distortions agree well qualitatively, but the calculate values significantly overestimate the measured values at the outer edges of the parts. This is partly due to the geometry of the part; given its large dimensions, a slight errors in distortion near the center would be magnified at the edges due to a parallax effect.

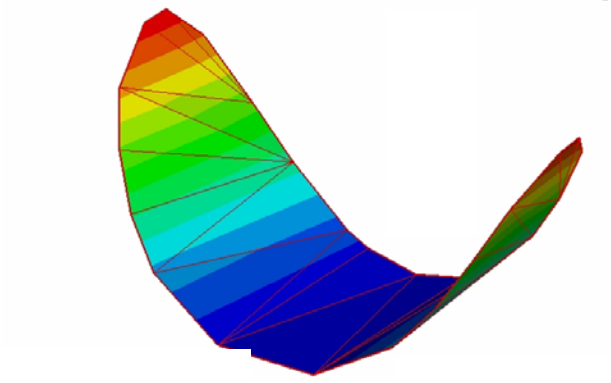

Fig 15: Measured distorted shape of Pressure Bulkhead

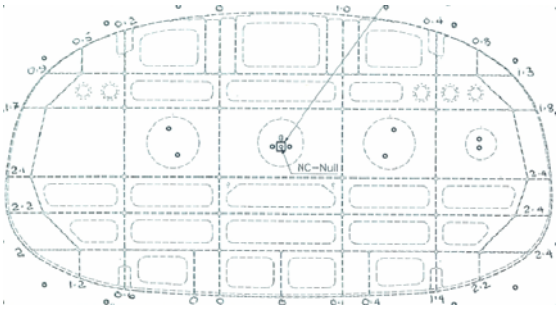

Fig. 16: Locations at which distortion was measured by feeler gauges

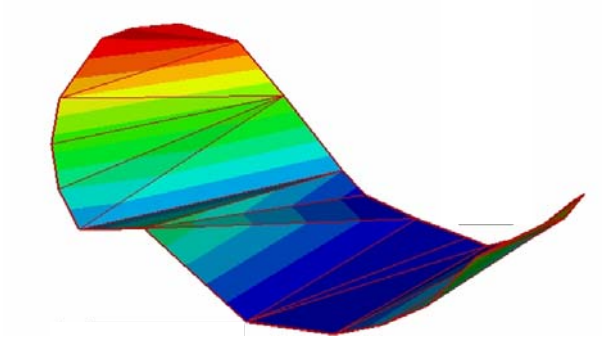

Fig. 17 Measured distorted shape of pressure bulkhead

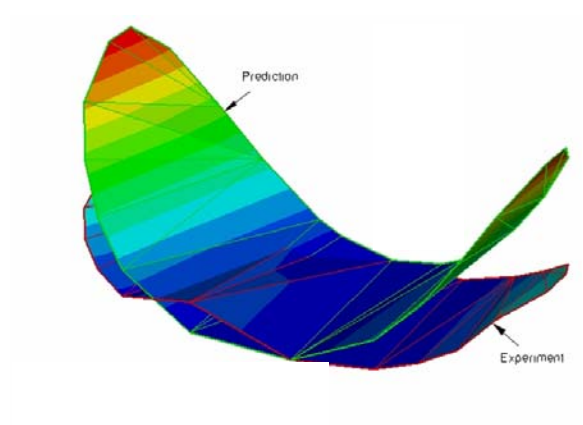

Fig. 18: Comparison of prediction versus measurement for Pressure Bulkhead

5. SUMMARY AND CONCLUSIONS

This paper summarizes a methodology for calculating distortions in thin-walled components due to both bulk and machining induced residual stresses. A tool path analysis program is used to determine the final part geometry, mesh the final part for distortion analysis, and apply stress components. Machining induced stresses are applied based on a database of values computed through finite element analysis for a range of representative cutting and tooling conditions. Measured bulk stresses in the parent billet are stored in a corresponding database. Preliminary validation of the bulk stress component for two aerospace parts is presented.

ACKNOWLEDGEMENTS

We are grateful to Martin Hand of EADS for valuable comments on this work, and for providing the fillet rib and pressure bulkhead data files and measurement data.

REFERENCES

[1] Stephenson, D. A., Agapiou, J. S., 2006, Metal Cutting Theory and Practice, Second Edition, CRC, Boca Raton, FL, 568-9

[2 C. Wiesner, C., 1992, "Residual Stresses After Orthogonal Machining of AISI 304: Numerical Calcuation of the thermal Component and Comparison with Experiments," *Metall. Trans*. **A 23** 989-996

[3] Shirakashi, T, Obikawa, T, Sasahara, H., Wada, T., 1993, "Analytical Prediction of the Characteristics Within Machined Surface Layer (1st Report, The Analysis of the Residual Stress Distribution," *J. Jpn. Soc. Precis. Eng.* **59** 1695-1700

[4] Shih, A. J., Yang, H. T. Y., 1993 "Experimental and Finite Element Predictions of Residual Stresses Due to Orthogonal Metal Cutting," *Int. J. Num. Meth. Eng.* **36** 1487-1507

[5] Liu, R., Guo, Y. B., 2000, "Finite Element Analysis of the Effect of Sequential Cuts and Tool-Chip Friction on Resdiual Stresses in a Machined Layer," *Int. J. Mech. Sci.* **42** 1069-1086

[6] Lundblad, M., 2002, "Influence of Cutting Tool Geometry on Residual Stress in the Workpiece," *Proc. 2002 Third Wave AdvantEdge User's Conference*, Atlanta, GA, Paper 7

[7] Shet, C., Deng, X., 2003, "Residual Stresses and Strains in Orthogonal Metal Cutting," *Int. J.Machine Tools Manuf.* **43** 573-587

[8] Marusich, T. D. and Ortiz, M., 1995, “Modeling and Simulation of High-Speed Machining”, *Int. J. Num. Meth. Eng* **38** 3675-94.

[9] Marusich, T. D., 2001, "Effects of Friction and Cutting Speed on Cutting Force," *Proc. IMECE* (ASME), Nov. 11–16, New York, Paper No. MED-23313.

[10] Sandstrom, D. R. and Hodowany, J. N., 1998, “Modeling the Physics of Metal Cutting in High-Speed Machining,” *Machining Science and Technology* **2** 343-353.

[11] Childs, T. H. C., 1998, “Material Property Needs in Modelling Metal Machining,” *Machining Science and Technology* **2** 303-316

[12] www.thridwavesys.com/products

[13] Prime M.B., Hill M.R. 2002, “Residual stress, stress relief, and inhomogeneity in aluminum plate” *Scripta Materialia* **46** 77-82